Marine and Petroleum Geology 97 (2018) 32–44

Contents lists available at ScienceDirect

Marine and Petroleum Geology

journal homepage: www.elsevier.com/locate/marpetgeo

Research paper

Coupling a frictional-cohesive cover and a viscous substrate in a discrete element model: First results of application to thick- and thin-skinned extensional tectonics

Stuart Hardy*

ICREA (Institució Catalana de Recerca i Estudis Avançats), Passeig Lluís Companys 23, 08010, Barcelona, Catalonia, Spain
Facultat de Geologia, Universitat de Barcelona, 08028, Barcelona, Catalonia, Spain

A B S T R A C T

Mechanical stratigraphy is now recognised as a fundamental control on the development of geological structures in the upper crust at a variety of different scales. This is perhaps never more apparent than when salt is part of the crustal section being deformed. The interaction of a ductile salt substratum and a brittle sedimentary cover is complex, but an understanding of it is essential both from an economic and academic standpoint. Here, I present first results of a discrete element model which combines a viscous (linear Newtonian) substrate and a frictional-cohesive cover. The modelling approach is firstly presented and experimental scaling to appropriate geological timescales discussed. The approach is then applied to 3 experiments simulating extensional deformation, two of which are thick-skinned and one is thin-skinned. Strain rates in all experiments are c. 10^{15} s^{-1}. The complex manner in which salt flows in the substrate and faults develop in the cover are illustrated and their linkage/evolution examined. Movement of the viscous substrate is the result of both Couette-type and Poiseuille-type flows and combinations thereof, whilst deformation in the cover takes the form of discrete, dilational faults which are not directly linked, or only soft-linked, to any sub-salt basement faults. Cover faults typically lose displacement towards, and tip out at, the cover-substrate interface. In addition, in models with a basement fault, the fault itself presents a growing and important no-slip boundary which significantly affects viscous flow. Implications for the timing/evolution of, and strain within, the resultant structures are discussed.

1. Introduction

Geological structures in sedimentary basins, or continental margins, are rarely simple and much of their complexity arises from the stratigraphic, and thus mechanical, heterogeneity of the crustal section being deformed. As a consequence of such mechanical heterogeneity, different sections of the sedimentary upper crust can deform in very different manners. This is particularly marked when salt is part of the stratigraphy (e.g., Stewart et al., 1996, 1997; Jackson and Lewis, 2016; Ge et al., 2016, Fig. 1a). This is because evaporite rocks, in particular salt, are much weaker than most other sediments. The viscosity of rock salt is subject to some debate but perhaps ranges between 1×10^{16} and 1×10^{18} Pa s (Jackson and Talbot, 1994; Withjack and Callaway, 2000). It will vary additionally depending on mechanical layering within the sequence itself and laterally. Regardless of the precise value, this allows it to flow over geological timescales and deform into the complex structures observed both in the field and in seismic. The involvement of salt in deformation has been studied through many geological and geophysical observations (e.g., Wu et al., 1990; Demercian et al., 1993; Marton et al., 2000; Rowan et al., 2000; Tari et al., 2002; Cartwright et al., 2012; Jackson and Lewis, 2016, Fig. 1a), principally as the result of hydrocarbon exploration. Significant thicknesses of salt occur in many passive continental margins and rifts (e.g., the Gulf of Mexico, many West African marginal basins, the Brazilian margin, the Nova Scotian margin, the North Sea). Continental margins typically contain a seaward thinning sedimentary wedge which often includes thick salt units. Moreover, they are characterised by a region of landward extension and a region of seaward contraction; which may be attributed to failure of the sedimentary overburden that accompanies the flow of the underlying salt (e.g., Worrall and Snelson, 1989; Koyi, 1996; Ge et al., 1997; Rowan et al., 2000). In many rift basins, such as the North Sea, evaporite rocks, including halite and gypsum, form an important, thick part of the pre-rift stratigraphy and can influence the structural and stratigraphic evolution of the rift (e.g., Hodgson et al., 1992; Stewart et al., 1999; Alves et al., 2002; Hudec and Jackson, 2007; Marsh et al., 2010; Duffy et al., 2013; Lewis et al., 2013). The evaporite

* ICREA (Institució Catalana de Recerca i Estudis Avançats), Passeig Lluís Companys 23, 08010, Barcelona, Catalonia, Spain.
E-mail address: stuart.hardy@icrea.cat.

https://doi.org/10.1016/j.marpetgeo.2018.06.026
Received 30 November 2017; Received in revised form 1 June 2018; Accepted 26 June 2018
Available online 28 June 2018
0264-8172/

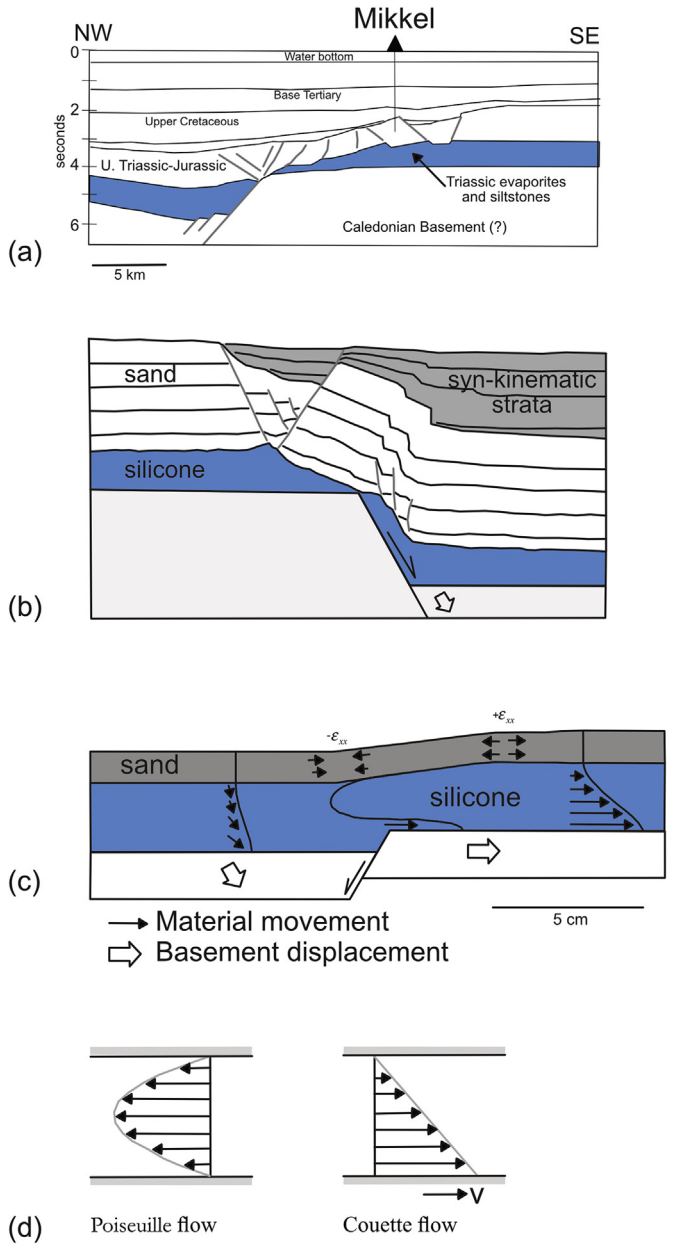

Fig. 1. (a) Line drawing of seismic section across the Mikkel structure, offshore Norway (redrawn from Withjack and Callaway, 2000), (b) Line drawing of an analogue experiment of deformation in cover above a ductile horizon overlying a 60° extensional fault (redrawn from Dooley et al., 2003) (c) Conceptual sketch summarising the interpreted displacement patterns and showing vector profiles representing material movement in an analogue experiment derived from PIV analysis (redrawn from Warsitzka et al., 2015), (d) Schematic illustration of Couette and Poiseuille flow.

units may fully or partially decouple the sub-salt deformation from that in supra-salt strata, giving rise to markedly different structural styles above and below the evaporite unit (Stewart et al., 1996, 1997; Withjack and Callaway, 2000; Richardson et al., 2005; Duffy et al., 2013, Fig. 1a and b). Salt also provides a ductile detachment layer allowing thin-skinned deformation to develop in the supra-salt strata when tilting induces gravitational sliding (e.g., Stewart and Coward, 1995; Stewart, 2007). The coupling and/or partitioning of deformation in such mechanically varied sections is complex, but a correct understanding of it is essential from both a scientific and an economic standpoint (e.g., Ferrill et al., 2017).

In addition to the examination of exposed examples, and seismically-imaged sections, in sedimentary basins, both analogue and numerical modelling have been used to gain insight into the controls on salt-involved deformation and the origin, styles and timing of resultant structures. Physical models have frequently employed weak, granular materials (dry sand or glass beads) to represent brittle rocks, and have produced results that bear a good, first-order, resemblance to many normal fault geometries observed in the upper crust (e.g., Horsfield, 1977; Vendeville, 1988; McClay, 1990). If salt is being considered, granular materials with different frictional properties or viscous polymer layers can be used to produce a wide variety of mechanical stratigraphies which, when subject to boundary conditions appropriate to salt tectonics, produce interesting and complex geometries (e.g., Vendeville, 1988; Dooley et al., 2003; Cartwright et al., 2012, Fig. 1b and c). Whilst model scaling, construction, running and analysis can prove difficult and time-consuming, such studies have given profound insight into salt tectonics (e.g. Vendeville, 1988; McClay et al., 2003; Dooley et al., 2003, 2007). Numerical modelling studies have also investigated the mechanisms that drive salt tectonics, including the buoyancy effects of relatively low-density salt buried beneath denser sediments (e.g. Podladchikov et al., 1993; Kaus and Podladchikov, 2001), differential loading of frictional sediments on top of a viscous salt unit (e.g., Last, 1988; Vendeville and Jackson, 1992; Poliakov et al., 1993; Jackson and Vendeville, 1994; Cohen and Hardy, 1996; Ge et al., 1997; Schultz-Ela and Walsh, 2001), to full margin-type studies (Gemmer et al., 2004, 2005).

Overall, these numerical and analogue modelling studies have shown that several end-member styles of deformation involving salt can occur: differential loading caused by varying overburden thickness creates a pressure gradient in the viscous salt and causes a channel Poiseuille flow to form (Fig. 1d; Turcotte and Schubert, 1982; Gemmer et al., 2004). With this end-member flow pattern, the overburden is stable and does not move horizontally (Last, 1988; Cohen and Hardy, 1996; Waltham, 1997). For larger differential overburden thicknesses, and hence larger pressure gradients, the overburden may become unstable and fail, initiating a drag-induced Couette-type flow in the viscous layer (Fig. 1d; Waltham, 1997). In nature, it is likely that salt flows in many types of environment involve both Couette and Poiseuille components, resulting in a velocity/displacement field that is a combination of both end-members (Gemmer et al., 2004; Warsitzka et al., 2015; Cartwright et al., 2012, Fig. 1c and d).

To complement these studies, here I use numerical modelling to investigate deformation of a crustal section composed of a brittle (frictional-cohesive) overburden underlain by a ductile (viscous) substrate, under extensional boundary conditions. Most numerical models (e.g., finite element, boundary element etc), whilst producing a detailed picture of evolving geometries, stress and strain, do not reproduce the important, smaller-scale structures in the sedimentary cover, particularly the faults, folds and fractures, seen in both the field and laboratory. This is partly a result of the limitations of many numerical codes (particularly continuum numerical techniques) in modelling spontaneous localisation and large displacement on faults but is also a result of model resolution (cf. Crook et al., 2006; Nollet et al., 2012). In contrast, discontinuum techniques (such as the discrete element method or smooth particle hydrodynamics) allow natural fault localisation and propagation, can incorporate a variety of rheologies, and replicate the complexity of smaller-scale structures seen in the field and laboratory (e.g., Saltzer and Pollard, 1992; Gray and Monaghan, 2004; Hardy, 2008). They also allow a detailed analysis of kinematics and strain (e.g., Cardozo and Allmendinger, 2009; Hardy, 2011). It is the discrete element technique that will be used in the study presented herein. Whilst discrete element models have previously been applied to over-pressured shale and salt tectonics, these studies did not include a *viscous* unit *per se* but rather modelled the mobile material as a very weak, non-cohesive, frictional layer (e.g., Dean, 2014; Dean et al., 2015) or a weakly-bonded elastic layer subject to global viscous damping necessary for numerical stability (Pichel et al., 2017). This paper presents an attempt to

combine a brittle (frictional-cohesive) overburden underlain by a ductile (viscous) substrate. The coupling between a viscous substrate and a frictional overburden and their numerical modelling is neither intuitive, obvious or straightforward, but a new approach is presented herein. Results under boundary conditions appropriate to thick- and thin-skinned extensional tectonics are presented and their implications discussed.

2. Methodology

The discrete-element technique used here has the advantage of relative ease in combining internal and external complicated, often abrupt, boundary conditions (see e.g. Hardy, 2008, 2011; 2016; Hardy et al., 2009). The discrete element code used here is ¨cdem2D¨, which is parallelised using OpenMP and was previously used to undertake a wide variety of structural geology modelling in both 2D and 3D (Hardy, 2008; Botter et al., 2014, 2016). The details of this code applied to frictional, cohesive materials can be found elsewhere (e.g., Hardy et al., 2009; Hardy, 2011, 2015) and the interested reader is referred to these publications. Here, I will focus on the inclusion of a viscous substratum in this modelling scheme and the issues associated with coupling it to a frictional-cohesive overburden. Preliminary results of the code were previously presented and published in extended abstract form (Valencia et al., 2016) but here the approach will be discussed in detail.

Discrete element models, in common with other numerical techniques, have both advantages and disadvantages when considering their application to a specific geological problem of interest. On the one hand, modelling of cover deformation to high strain is an ideal candidate for the application of the discrete element technique as it is well-suited to studying problems in which discontinuities (shear-zones, faults, fractures etc) are important. It allows deformation involving unlimited relative motions of individual elements and complex, abrupt boundary conditions (Cundall and Strack, 1979; Finch et al., 2004: Egholm et al., 2007; Hardy, 2008, 2011; Thompson et al., 2010). However, one disadvantage of the technique lies in the necessary, but tedious and time-consuming, calibration of micro-particle parameters to emergent physical properties (cf. Egholm et al., 2007; Botter et al., 2014). Similarly, the sensitivity of models results (e.g. the precise location and timing of faulting, number of faults etc) to subtle initial differences in, e.g., assembly packing is well-known (cf. Abe et al., 2011). The interaction of many tens of thousands of particles, both locally and globally, also leads to situations wherein our ability to explain precisely *why* a particular fault or fracture grew at the expense of a neighbouring one is limited. Such issues also exist in analogue modelling where repeated experiments under the same boundary conditions are reasonably reproducible but not in the finer details of the fault and fracture systems (e.g., van Gent et al., 2010). Computational limitations on element size and/or model resolution, whilst important previously, are now no longer a particular concern due to recent rapid advances in computational power and the parallelisation of many discrete element codes.

Here, I model the substratum of salt as a simple, linear Newtonian fluid. Such a fluid is one in which the viscous stresses arising from its flow, at every point, are linearly proportional to the local strain rate — the rate of change of its deformation over time. That is equivalent to saying that these forces are proportional to the rates of change of the fluid's velocity vector as one moves away from the point in question. More specifically, a fluid is Newtonian only if the tensors that describe the viscous stress and the strain rate are related by a constant viscosity tensor that does not depend on the stress state and velocity of the flow. Newtonian fluids are the simplest mathematical models of fluids that account for viscosity and are named after Isaac Newton, who first postulated the relation between the shear stress and shear strain rate for such fluids in differential form

$$\tau = \mu \frac{du}{dy} \quad (1)$$

Where

τ is shear stress
μ is a scalar constant of proportionality, the dynamic viscosity of the fluid
$\frac{du}{dy}$ is the shear strain rate, the derivative of the velocity component that is parallel to the direction of shear, relative to the perpendicular direction

Equation (1) is known as the Newtons Law of Viscosity. This equation describes a Linear Newtonian viscous fluid with constant viscosity. The incorporation and calculation of such viscous contact stresses in 2 dimensions, and thus forces, in the discrete element model is a moderately straightforward task.

2.1. Viscosity scaling and viscous-brittle coupling

Unfortunately, whilst *calculation* of viscous and frictional forces in the numerical model is moderately straightforward, the incorporation of different constitutive descriptions of behaviour *can* be hampered by technical difficulties induced by the distinct nature of the time-independent (frictional) versus time-dependent (viscous) mechanisms, and the abrupt/discontinuous change of material behaviour across any sediment-salt interface(s).

A particular issue revolves around the *extremely* small time-steps necessary in many discrete element simulations to both ensure both numerical stability and high resolution, combined with the extremely long (geological) timescales over which the modelled materials must be simulated and deformed (cf. Gemmer et al., 2004, 2005). Typically discrete element models have time-steps of the order of 0.001s or less depending on element size, density, elastic modulus, etc. A consequence of this is that we often require many, many millions of calculation time-steps to achieve, for example, a desired final fault displacement. For frictional materials time is independent of deformation and, with today's computing power and parallelisation, as long as numerical stability is ensured, such large numbers of time-steps do not present any real computational problem. However, with viscous materials time *is* important and deformation must take place over geologically appropriate timescales. Obviously, such small time-steps cannot be used to model geological timescales (100s of thousands to 10s of millions of years) and therefore some approach to model scaling must be adopted. As proposed by Last (1988), in problems where deformation is essentially constrained by slow viscous flow, scaling of viscosity is an appropriate technique. The model viscosity can be scaled (decreased) to speed up the calculation process providing that *inertial* forces are small in comparison to *viscous* forces. An appropriate measure of this is the Reynolds number (Re), a dimensionless number that gives a measure of the ratio of inertial forces to viscous forces for given flow conditions. The Reynolds number is an important parameter that describes whether flow conditions lead to laminar or turbulent flow. Laminar flow occurs at low Reynolds numbers, where viscous forces are dominant, and is characterised by smooth, constant fluid motion; turbulent flow occurs at high Reynolds numbers and is dominated by inertial forces, which tend to produce chaotic eddies, vortices and other flow instabilities.

The Reynolds number is defined as:

$$\mathrm{Re} = \frac{\rho v L}{\mu} \quad (2)$$

where:

ρ is the density of the viscous fluid (kg/m^3)
v is a characteristic velocity of the viscous fluid (m/s)
L is a characteristic length scale (m)

μ is the dynamic viscosity of the viscous fluid (Pa.s).

For a scaled system, the coefficient of viscosity simply becomes

$$\mu^s = \mu/\lambda \quad (3)$$

Where:

λ is the scaling factor

In a system under quasi steady-state conditions, such a scaling will simply increase the computed velocities by the same factor

$$v^s = \lambda \cdot v \quad (4)$$

As such, and combining Equations (2)–(4), it is clear that the Reynolds number for the scaled computations becomes

$$\mathrm{Re}^s = \lambda^2 \mathrm{Re} \quad (5)$$

Thus, the scaling factor should be chosen such that the resultant, *scaled*, Reynolds number, Re^s, is « 1. For the system under consideration in this paper, with a characteristic length scale of 1000 m, density of salt of c. 2200 kg/m^3, flow/displacement velocities of c. 0.05 m/s and a viscosity of c. 5×10^8 Pa s - the calculated *scaled*, Reynolds number, Re^s is c. 2×10^{-4} (see below and Table 1). Thus, for these parameters, the Re^s is « 1 and the scaled viscous flows remain steady, smooth and laminar. Therefore, if we use a scaling factor, lambda, λ of 10^9 the natural viscosity is c. 5×10^{17} Pa s and the real world Reynolds number, Re, is c. 2×10^{-22}. Models are run for c. 0.23 days of model time - which, with this scaling factor λ of 10^9, scales to c. 634 ka in real geological time (see Table 1). Note that these natural parameters are obviously subject to some uncertainties, given that both salt viscosity and strain rate during salt flow are not well constrained and may vary over several orders of magnitude (Jackson and Talbot, 1994).

A second technical issue when dealing with viscous layers is the implementation of no-slip boundary conditions. The no-slip condition for viscous fluids assumes/implies that at any solid boundary, the fluid will have zero velocity *relative* to that boundary. This condition is required both at the interfaces between external model boundaries and at the internal sedimentary cover-viscous substrate interface. Luckily, this is not a great technical concern in discrete element models, and one can easily specify that a particular boundary is no-slip, without creating technical difficulties or instabilities.

2.2. Model parameters, set-up and boundary conditions

Three different experiments are considered herein, all contain a viscous lower section 1000 m thick (representing salt) and an overlying frictional-cohesive section 1750 m thick (representing a brittle, sedimentary cover). The first example considered contains a basement normal fault dipping at 30° (Fig. 2a), the second example considers deformation above a keystone-type graben with 2 opposing 60° faults (Fig. 2b), whilst the third example is thin-skinned in which the model is tilted by 5° and then subject to extension via its right-hand wall (Fig. 2c). These model designs were chosen to illustrate the range of settings and boundary conditions that the approach can handle; they are not unique or intended to replicate specific natural examples. The model in the keystone example is longer in order to accommodate the 2 faults and ensure that they are neither too close to each other or the model boundaries. In all cases the upper section is marked/coloured using initially horizontal layers whilst the lower section is coloured using vertical layers, in order to emphasise their different deformation styles. Both horizontal and vertical marker layers are initially 60 m thick. The models represent the crustal section (both salt and sediments) as a densely packed assemblage of c. 47,000 (Expts 1&3) or c. 94,000 (Expt 2) variably-sized, circular elements. Element radii range from 6.25 to 15.625 m (average radius 9.71 m) and their density is 2200 kg/m3. These elements obey Newton's equations of motion and interact with each other under the influence of gravity. Elements are not bonded to their neighbours and experience either Mohr-Coulomb frictional or viscous contact interactions with their neighbours (see Finch et al., 2004 and Hardy et al., 2009 for a full description of the modelling approach).

Table 1
Experimental and equivalent, scaled natural model parameters, for standard strain rate experiments.

	Numerical Model	Natural Example using viscosity scaling of 10^9
Salt Layer Thickness (m)	1000	1000
Salt Layer Density (kg/m^3)	2200	2200
Salt Layer Viscosity (Pa.s)	c. 5×10^8	c. 5×10^{17}
Total Time (days)	0.23	n/a
Total Time (Yrs)	0.000634	6.34×10^5
Displacement Rate (m/s)	0.05	5×10^{-11}
Displacement Rate (m/ka)	n/a	1.58
Reynolds Number (Re)	0.00022	2.2×10^{-22}
Cover Layer Angle of Friction (deg)	38	n/a
Cover Layer Cohesion (MPa)	2.5	n/a
Cover Layer Density (kg/m^3)	2200	n/a

In discrete element models such as that used here the parameters such as strength, coefficient of friction or viscosity of an assemblage are emergent properties and do not relate directly to micro-properties. They are typically assessed through the use of angle of repose and unconfined/confined biaxial numerical tests (cf. Oger et al., 1998; Finch et al., 2004; Holohan et al., 2011; Botter et al., 2014). Using such tests, the overlying frictional-cohesive cover used here has been found to have a bulk coefficient of friction (μ) of c. 0.79 (internal angle of friction (ø) of c. 38°) and a cohesion (C) of ~2.5 MPa (Table 1). These values lie within the ranges reported for natural rock masses at a metric scale and are much smaller than those typically derived from centimetre-scale laboratory samples (cf. Schultz, 1996; Strayer et al., 2004; Holohan et al., 2011). The underlying, viscous substrate has a nominal dynamic viscosity (μ) of 5×10^6 Pa s, and this together with the numerical damping used in the model leads to an *effective* dynamic viscosity of c. 5×10^8 Pa s. Using a scaling factor, lambda, λ of 10^9 (see above and Table 1) thus allows us to model mobile substrates with a viscosity of c. 5×10^{17} Pa s.

Displacement on the basement fault or sidewall is incremented by 0.0001 m per time-step (0.002 s) to achieve a total displacement of 1000 m in both the case of the basement fault models and the titled model. Models are run for c. 0.23 days of *model* time, which scales to c. 0.634 Ma in real geological time (see Table 1). The displacement rate scales to c. 1.5 m/ka, well within reported fault displacement rates (see Hardy, 1994). For all three models the scaled strain rates are c. 10^{15} s^{-1} consistent with reported geological strain rates (e.g., Baldwin et al., 2003). The applied basement fault or wall displacement is transmitted directly to the cover, changing local element interactions and thus contact forces. As a result of this boundary displacement, the internal elements are advanced to their new positions within the model by integrating their equations of motion using Newtonian physics and a velocity-Verlet based numerical scheme (cf. Mora and Place, 1993). Element positions are saved during experiments to allow a detailed, high-resolution analysis of geometry, displacement and strain (cf. Cardozo and Allmendinger, 2009). The numerical code used has been parallelised using OpenMP and has been thoroughly tested and verified against the serial version (cf. Chapman et al., 2007; Hardy, 2015). Typical experiments like those discussed here take ~5–7 days of machine (calculation) time on a desktop machine with two 6-core Intel Xeon (X5650–2.66 GHz) processors allowing 24 computational threads.

For each experiment discussed herein many different models have been run with parameters similar to those described below. However, the *specific* experiments discussed are representative of the structural

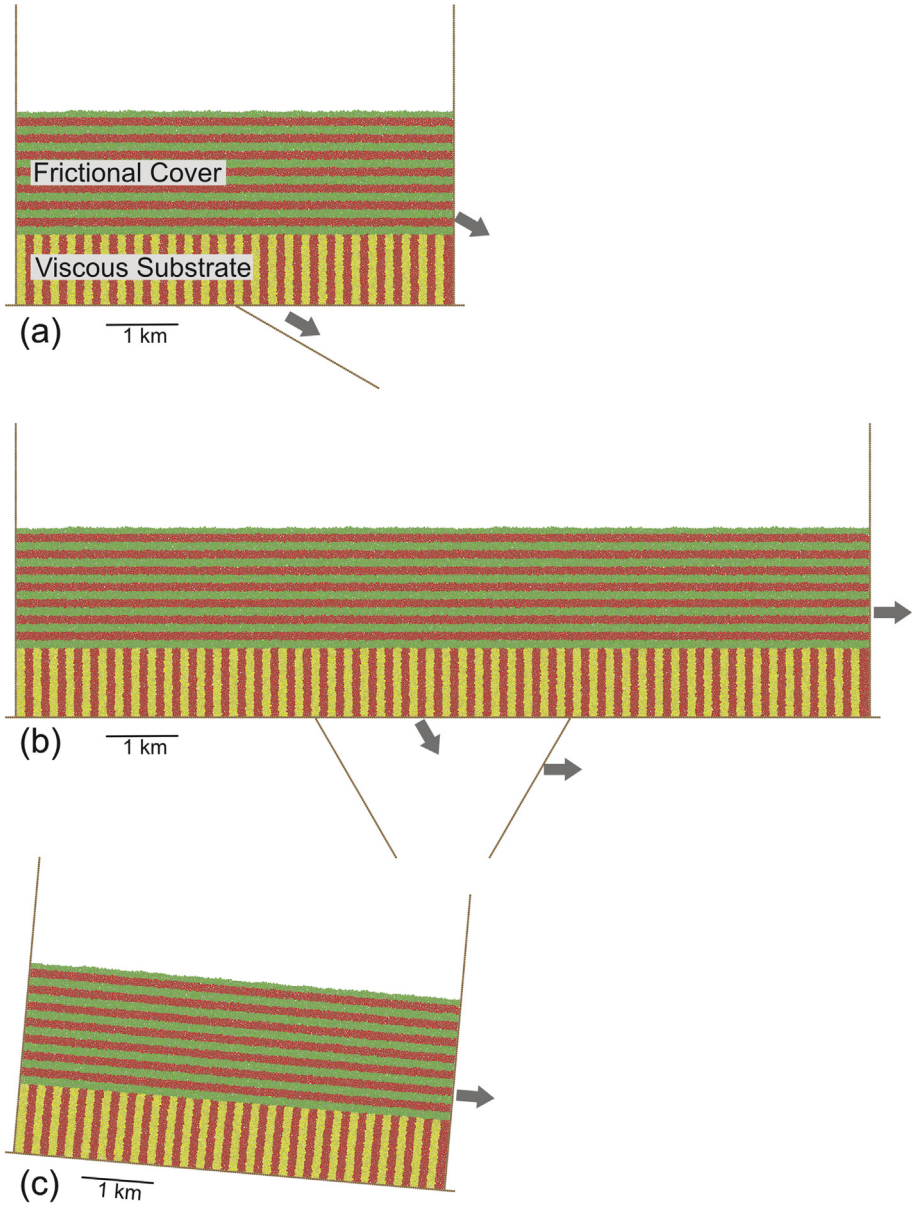

Fig. 2. Initial and boundary conditions of the 3 experiments discussed in this paper. In all cases the cover contains a viscous lower section 1000 m thick representing ductile salt, and an overlying frictional-cohesive section 1750 m thick representing a brittle, sedimentary overburden. The upper section is marked/coloured using initially horizontal layers whilst the substratum uses vertical layers, to emphasise their different deformation styles. Both horizontal and vertical marker layers are initially 60 m thick. Arrows indicate boundary displacements applied.

evolution typically observed under these boundary conditions in that they contain the reproducible, characteristic features seen in many models that were run. The important scientific message to be taken away is not the precise location of an individual fault, but rather the distinctive, repeatable patterns and sequences of structural behaviour that emerge from multiple experiments that are represented by the three experiments shown here.

2.3. Experiment 1

The first scaled 2D numerical experiment reported here considers a 6.25 km by 2.75 km section of the upper crust, subject to displacement on a single, blind 30° normal fault centrally located at its base (Figs. 2a and 3). Results are shown after 100, 250, 500, 750 and 1000 m displacement on the basement fault. Also shown is the incremental shear strain calculated over the previous 50 m basement fault displacement at each stage.

An overview of the experimental results allows us to extract some general, large-scale features: the lack of localisation/faulting within the viscous (ductile salt) unit, discrete (dilational) faulting in the frictional-cohesive (brittle cover) unit, and the flow of salt in both the hanging wall and the footwall of the basement fault. Model evolution can be summarised as follows: after 100 m of displacement on the basement fault (Fig. 3a), it can be seen that there is some flow of the salt (as evidenced by deformation of originally vertical markers) and the subtle development of a steep extensional fault/dilational fracture in the upper part of the frictional cover; there is no visible faulting within the viscous unit. In a *general* sense, the overburden fault is spatially related to the deeper fault but there is no direct linkage, and faulting does not initiate at the projection of the basement fault into the brittle cover. As can be seen from the incremental shear strain, deformation within the salt unit is quite widespread and diffuse. The flow of salt is subtle but is towards the downthrown side of the fault. It is concentrated in a wide zone above the fault tip, although there is also some minor flow in the

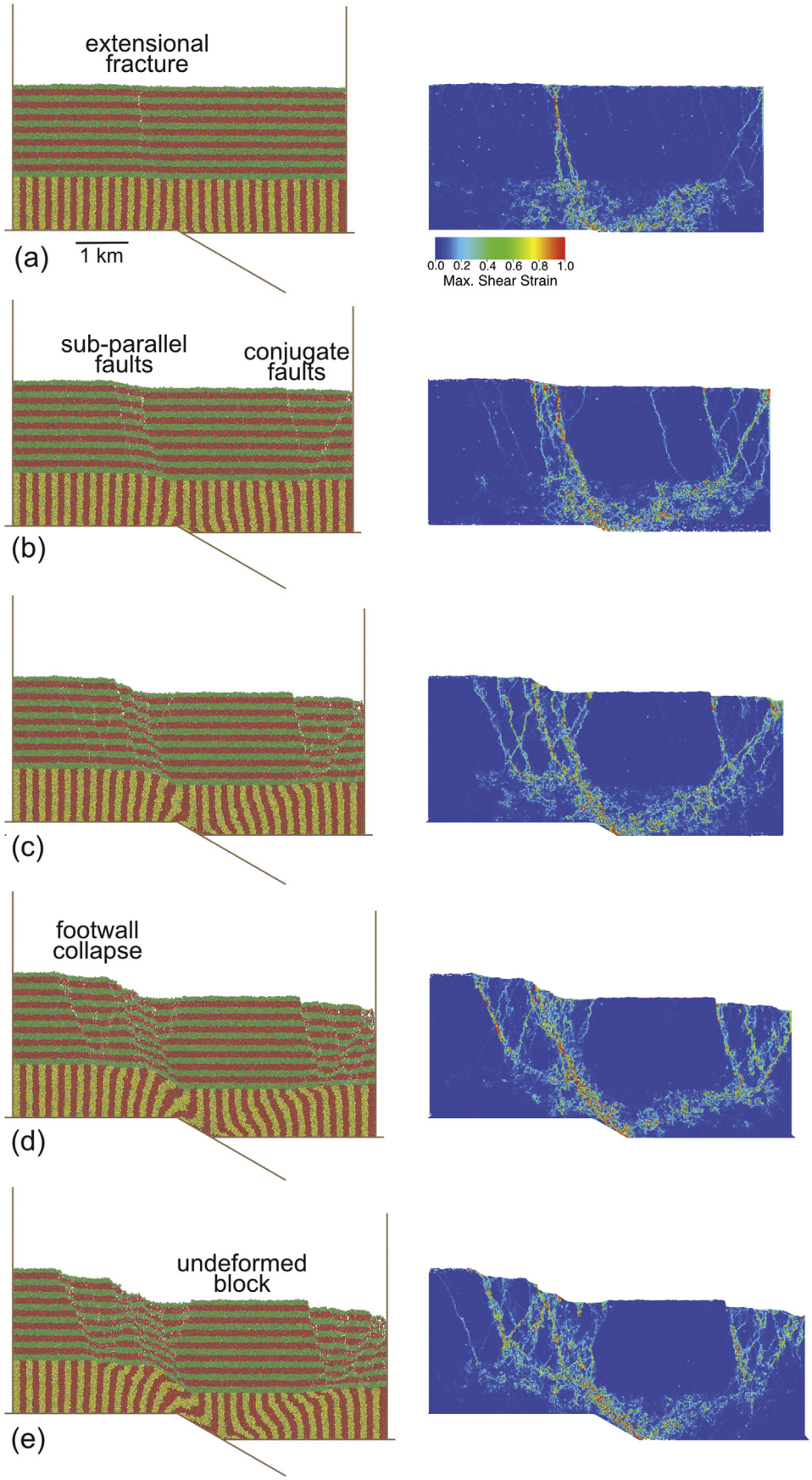

Fig. 3. Experiment 1: a centrally located basement normal fault dipping at 30° deforms a viscous lower section 1000 m thick (representing ductile salt) and an overlying frictional-cohesive section 1750 m thick representing a brittle, sedimentary overburden. Model geometry shown after 100, 250, 500, 750 and 1000 m displacement on the basement fault.

hanging wall towards the fault. After 250 m of displacement on the basement fault, the zone of salt flow is somewhat wider and, concurrently, the cover deformation has become more complex (Fig. 3b). Salt flow now occurs over a wide region of the footwall and is directed towards the hanging-wall, whilst in the hanging-wall there is a subtle flow of salt *towards* the growing fault plane. Discrete, dilational faulting continues in the cover with several, sub-parallel, faults forming above the basement fault; in addition, more faulting now occurs in the hanging wall (Fig. 3b). Of particular note is the development of 2 conjugate normal faults adjacent to the right-hand end-wall. This pattern of deformation continues after 500 m displacement. Flow in the salt is complex, more widespread but continuous (Fig. 3c). At this stage, apart from close to the right-hand wall, much of the normal faulting is in the footwall of the basement fault. It is also now that we see the development of a central block within the cover which is essentially undeformed. After 750 m deformation has propagated even further into the footwall (with a conjugate normal fault set developing) and salt flow is complex, but emphasises the dominant flow of salt from footwall to hanging-wall, and minor flow of salt in the hanging-wall towards the fault (Fig. 3d). The main cover fault can be seen to be *soft-linked* to the basement fault, although there is no discrete faulting *per se* in the salt. Analysis of individual, major, faults in the cover show them to be active together. The final stage of deformation shows this trend to continue with a wide zone of deformation in the cover. The effect of a growing, new, no-slip boundary (the fault plane) is very clear in this experiment. In addition, the salt layer has thinned to approximately 400 m near the edge of the footwall block and faults in the brittle overburden are now more closely aligned with the basement fault beneath the salt (Fig. 3e).

2.4. Experiment 2

The second scaled 2D numerical experiment reported here considers a 12.50 km by 2.75 km section of the upper crust (essentially twice as wide as Expt. 1), subject to displacement on 2 blind, opposing, 60° normal faults centrally located at its base (Fig. 2b; Fig. 4). Displacement on these 2 faults produces a symmetric, keystone-type, graben in the basement. This experiment will highlight the importance of specific boundary conditions when modelling salt in a setting such as this. In order to simulate a keystone that drops down due to space created by moving a right-hand wall outwards, the left-hand part of the model is kept static, the central keystone is displaced parallel to the left-hand fault, whilst the right-hand part of the model moves horizontally to the right at the correct rate to produce a symmetric graben (Fig. 2b). Both these styles of boundary condition (single fault equivalent to left hand side of model and keystone block style of full model) have been used in previous analogue modelling studies (Dooley et al., 2003; Warsitzka et al., 2015, Fig. 1b and c) and their effect on the resultant pattern of deformation will be shown here. Results are shown after 100, 250, 500, 750 and 1000 m displacement on the basement faults. Also shown is the incremental shear strain calculated over the previous 50 m fault displacement at each stage.

An overview of the experimental results allows us to observe (as before) several general, large-scale features: the lack of localisation within the viscous unit, discrete (dilational) faulting in the frictional unit, and the flow of salt from both footwall blocks towards the central graben. However, the most striking feature is the asymmetric nature of deformation in this experiment, with a wide zone of extensional faulting in the brittle cover above the *righthand* footwall block and a more limited zone of deformation above the *lefthand* footwall block. Whilst this might not be surprising if one analyses the model set-up, it emphasises the importance of boundary conditions when modelling even single faults. Model evolution can be summarised as follows: after 100 m deformation on the basement faults there is an initial almost symmetric flow of salt towards the graben with only gentle flexing of the brittle cover and no visible faulting (Fig. 4a). After 250 m displacement, we see the development of both subtle rotational “reverse”, and more prominent normal, faults in the frictional cover. Even at this stage the cover deformation is asymmetric with widely distributed normal faulting above the righthand footwall block and only minor faulting above the lefthand footwall block (Fig. 4b). Flow patterns in the salt reflect this asymmetry in deformation. This pattern of asymmetry continues and by 500 m the left side continues to develop as before whilst the right side changes dramatically with further propagation of deformation into the footwall with prominent conjugate faulting developing. The flow of salt is now also asymmetric with a limited zone of deformation above the lefthand basement fault, whilst shear-flow dominates above much of the righthand footwall block (Fig. 4c). Note also the viscous shear of the salt between the downthrown keystone block and the overlying, undeformed central cover section. This pattern continues after 750 and 1000 m displacement, with clear development of conjugate normal faults and mini-graben above the righthand footwall block. At this stage, faulting also begins to propagate into the lefthand football block as it collapses (Fig. 4d and e). In addition, the salt layer has thinned to approximately 325 m immediately above the basement fault tips (Fig. 4e).

2.5. Experiment 3

The third scaled 2D numerical experiment reported here considers the same 6.25 km by 2.75 km section of the upper crust as in Experiment 1 *but without any basement fault*, however it is now subject to an initial tilt of 5° and then extension via its right-hand end-wall (Fig. 2c; Fig. 5). As before, results are shown after 100, 250, 500, 750 and 1000 m displacement on the right-hand wall, along with the incremental shear strain calculated over the previous 50 m of wall displacement at each stage.

As before we can observe several general, large-scale features: the lack of localisation within the viscous unit, discrete (dilational) faulting in the frictional unit, and the flow of salt downslope towards the moving right wall. Model evolution can be summarised as follows. After 100 m of end-wall displacement one can observe the beginning of downdip salt flow towards the bottom righthand corner over much of the viscous unit. Salt flow is very widely distributed and, from the incremental shear strain, can be seen to not be localised (Fig. 5a). There is no visible faulting in the cover but strain can be seen to be localised in the shear strain plot at the right end-wall and in the central part of the brittle cover. After 250 m of end-wall displacement, two major, planar extensional faults have developed near the righthand edge of the model, with more minor faulting upslope (Fig. 5b). After 500 m of end-wall displacement, extensional faulting has migrated upslope with the development of a series of subparallel, synthetic (downslope) normal faults. There is clearly a dominant, downslope fault vergence and individual rotated fault-blocks are tilted upslope by 3–5° (Fig. 5c). In addition, minor (upslope) antithetic faulting has initiated with the formation of a small graben towards the right-hand edge of the model (Fig. 5c). Salt flow is now visible over much of the model but is at its most complex at the right-hand edge of the model. After 750 m of end-wall displacement the same pattern of deformation is observed. The graben at the right hand end of the model continues to grow (Fig. 5d) at the same time as antithetic faulting migrates upslope. Of particular note is the development of an essentially undeformed, sinking block squeezing out the underlying salt at the right-hand end of the model. The influence of model edges and boundary conditions will be returned to in the discussion. This pattern of deformation continues up to 1000 m of end-wall displacement, producing the final geometry (Fig. 5e).

3. Discussion of results

The experiments presented in this paper, as expected, illustrate well the very different manners in which a ductile substrate and a brittle overburden respond to imposed (extensional) boundary conditions. Diffuse, ductile deformation predominates in the viscous salt layer

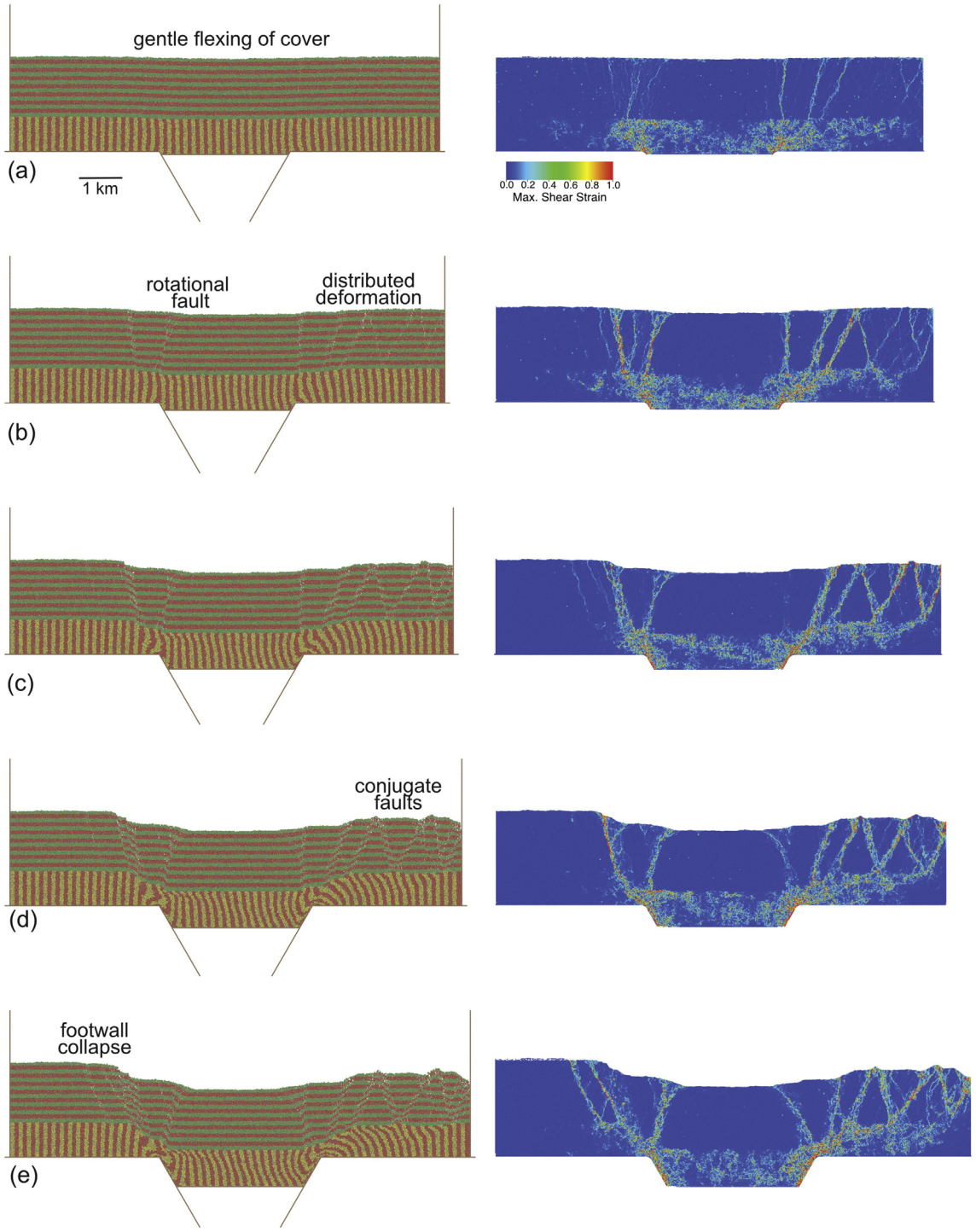

Fig. 4. Experiment 2: deformation above a keystone type graben with 2 opposing 60° faults. This model is wider than Expt. 1 but all other parameters are identical. Model geometry shown after 100, 250, 500, 750 and 1000 m displacement on the basement fault.

whereas localised, dilational faulting occurs in the frictional overburden layer (e.g., Fig. 3b; Fig. 5c). However, although the two layers are physically in contact with each other, the manner in which deformation passes from one to another, and links to that in the basement, is not straightforward. Faults in the brittle cover typically lose all displacement/expression at the salt-cover interface (i.e., they tip out) as localised deformation passes to distributed flow in the underlying salt (Figs. 3–6). The interface *per se* is never offset by faulting but clearly can develop moderate relief as a result of deformation and flow above and below it. As such, for the thickness of salt used in these experiments, while there is often a *spatial* relationship, there is typically no *direct* linkage between the basement fault(s) and the faults above the salt in the overburden. Thus, the systems are probably best described either as being unlinked or soft-linked. However, when the salt layer thins significantly near the edge of the footwall block, the faults in the overburden are more closely related to those beneath the salt, however there is still no discrete faulting *per se* within the salt (see, e.g., Figs. 3e and 4e). However, initially thinner salt layers in such models would be expected to produce greater linking between deformation in basement and cover (see below). In general, the model results compare well with

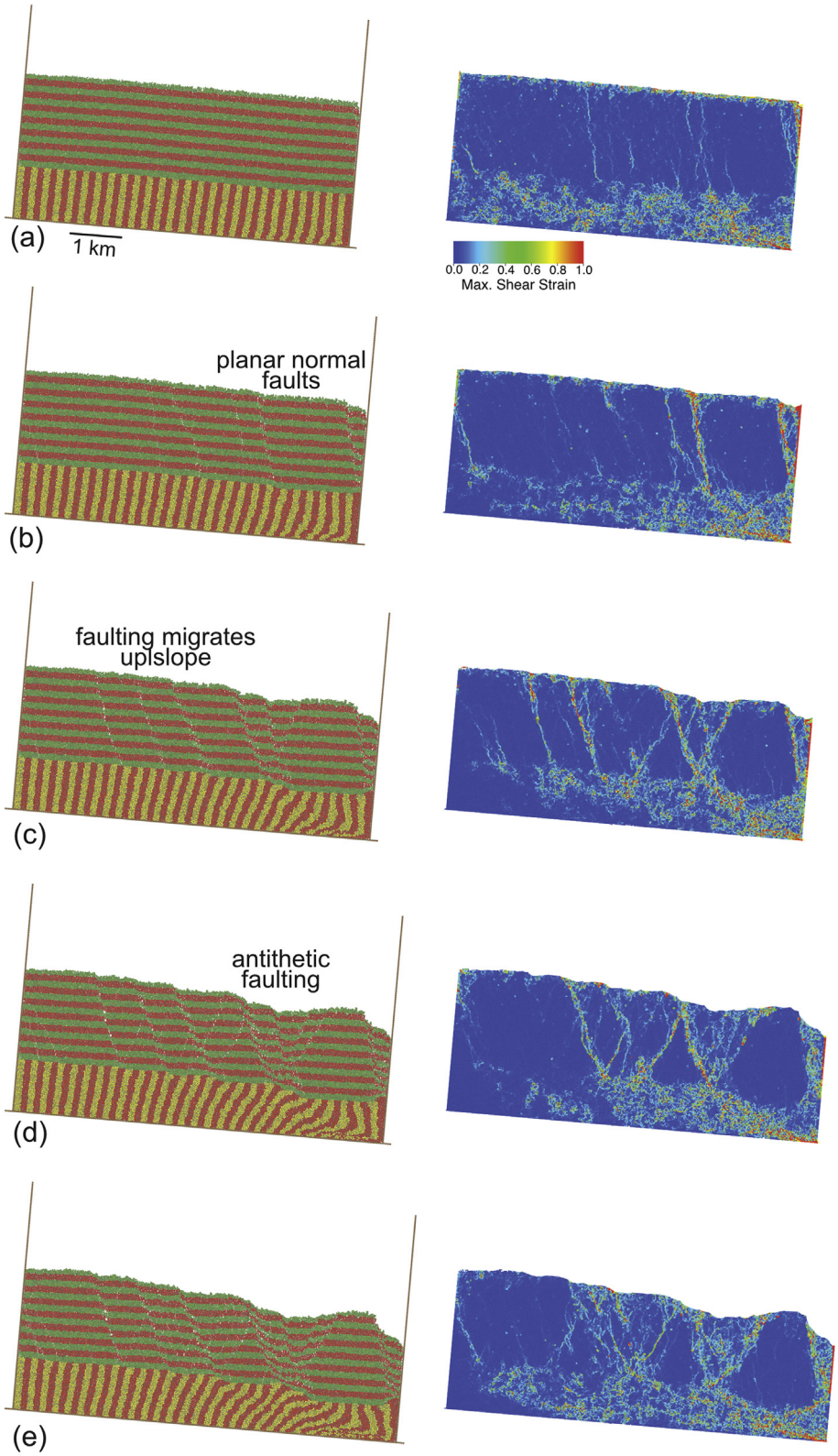

Fig. 5. Experiment 3: thin-skinned and in this experiment the model is tilted by 5° and then subject to extension via its right-hand wall. Model geometry shown after 100, 250, 500, 750 and 1000 m displacement on the basement fault.

those seen both in nature and in analogue experiments (cf. Fig. 1a,b,c). They show many key/characteristic features observed when a thick salt unit lies between basement and cover. These include: a clear decoupling of deformation between basement and cover, widely-distributed graben-like conjugate fault systems above the basement footwall, rotational "reverse" faults in downthrown cover blocks and, in the case of the inclined base model, tilted fault blocks with approximately constant spacing and downslope vergence. All of these observations give us some confidence in the fidelity of the modelling code and the applicability of the modelling results.

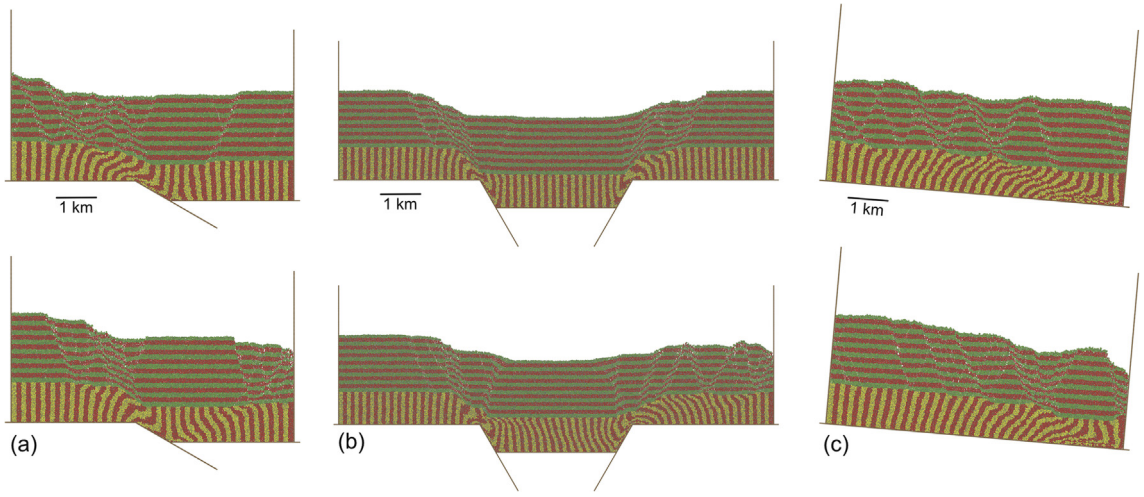

Fig. 6. Final geometries after 1000 m fault and endwall displacement for Experiments 1, 2 & 3 discussed in text (Figs. 3–5) run at the standard strain rate (c. 10^{15} s^{-1} bottom row) and equivalent experiments run at a strain rate that is 5 times lower (top row). All other model parameters are identical. Note the reduction of edge effects in all models and greater localisation of strain in cover.

The experiments also demonstrate the important role of boundary conditions in the models and, by analogy, in nature. No-slip boundary conditions occur at the salt-base, salt-top and at the end-walls. They condition much of deformation seen in the experiments. This is only to be expected when considering a viscous, Newtonian material. As indicated by the (initially) vertical markers, the strain patterns in the viscous layer can be described as shear flow (Couette flow; Fig. 1d) when they occur between simple, almost planar, boundaries such as those seen in the tilted model, or the central hanging wall block and the horizontally moving footwall in the keystone model (Fig. 4; Fig. 5). However when the viscous layer flows towards a subsiding basement block (e.g., Figs. 3 and 4) or a moving end-wall (Fig. 5), the (initially) vertical markers in these zones show a more parabolic shape, which is characteristic of channelized Poiseuille-type flow (Fig. 1d). In these cases Poiseuille-type flow occurs where there is either important basement relief and/or where there is significant thinning (relief) of the cover due to faulting and endwall movement. In models with a basement fault, the rigid fault plane also introduces a new, growing, no-slip boundary which can lead to complex salt flow towards, and drag along, the fault (Figs. 3e and 4e). In general, it can be observed that salt flow is quite complex; flow patterns typical of both Couette and Pouseueille flow, and combinations thereof, are seen (cf. Fig. 1c and d).

As viscous deformation depends explicitly on strain rate (cf. Eqn. (1)), it will prove useful to examine models identical to those presented above but run with a significantly lower strain rate. These lower strain rate models will also allow us to examine the effect of model boundary conditions (and thus edge effects) on deformation style, e.g., the model asymmetry observed in the case of the keystone experiment. I choose a strain rate that is 5 times lower than the previously presented results. Displacement on the basement fault or sidewall is now incremented by 0.00002 m per time-step (0.002 s) to achieve a total displacement of 1000 m in both the case of the 2 basement fault models and the titled model. Models are run for c. 1.16 days of model time, which with a scaling factor, lambda, λ of 10^9 translates to c. 3.17 Ma in real geological time and leads to a much lower Reynolds numbers (see Table 2). The displacement rate scales to c. 0.315 m/ka, well within reported fault displacement rates (see Hardy, 1994). For all three models the scaled strain rates are c. 10^{15}-10^{16} s^{-1}, still consistent with reported geological strain rates (cf. Baldwin et al., 2003). In Fig. 6 the final geometries (after 1 km displacement) of both the original and lower strain rate experiments are shown. What can be seen is that in these lower strain rate experiments the effect of the boundary conditions is reduced but it does not entirely disappear. For example, with the lower strain rate, in the 30° experiment the righthand wall graben is no longer present and is replaced by a prominent antithetic fault (Fig. 6a). In addition, faulting in the cover is now more distributed and is not clearly linked to the basement fault. In the keystone experiment the lower strain rate reduces some of the asymmetry in deformation but it is still present (Fig. 6b). However, there is also a noticeable reduction in reverse (rotational) faulting above the basement faults, and no viscous shear (Couette flow) in the salt above the central, downthrown block. In the mobile righthand wall experiment deformation is broadly similar to that seen in the standard strain rate experiment, although the role of antithetic faulting is now more apparent across much of the model (Fig. 6c), producing conjugate fault sets and a set of graben across the model rather than tilted fault blocks. However, in all cases, what is clear is the key role of strain rate (or equivalently, viscosity) on the nature of deformation both in the mobile substrate and the overlying brittle cover. In particular, these experiments emphasise the importance of edge effects when modelling such materials. Clearly edge effects are difficult to completely eliminate in either analogue or numerical models, but models such as these allow us to distinguish between edge effects and real-world behaviour.

A final set of models will now be shown in order to illustrate the importance of initial salt thickness on linkage between deformation in the basement and cover (Fig. 7). Shown here are the three final model configurations (after 1000 m displacement) of experiments with a 65°

Table 2
Experimental and equivalent, scaled natural model parameters, for lower strain rate experiments.

	Numerical Model	Natural Example using viscosity scaling of 10^9
Salt Layer Thickness (m)	1000	1000
Salt Layer Density (kg/m^3)	2200	2200
Salt Layer Viscosity (Pa.s)	c. 5×10^8	c. 5×10^{17}
Total Time (days)	1.16	n/a
Total Time (Yrs)	0.00317	3.17×10^6
Displacement Rate (m/s)	0.01	1×10^{-11}
Displacement Rate (m/ka)	n/a	3.15×10^{-1}
Reynolds Number (Re)	0.000044	4.4×10^{-23}
Cover Layer Angle of Friction (deg)	38	n/a
Cover Layer Cohesion (MPa)	2.5	n/a
Cover Layer Density (kg/m^3)	2200	n/a

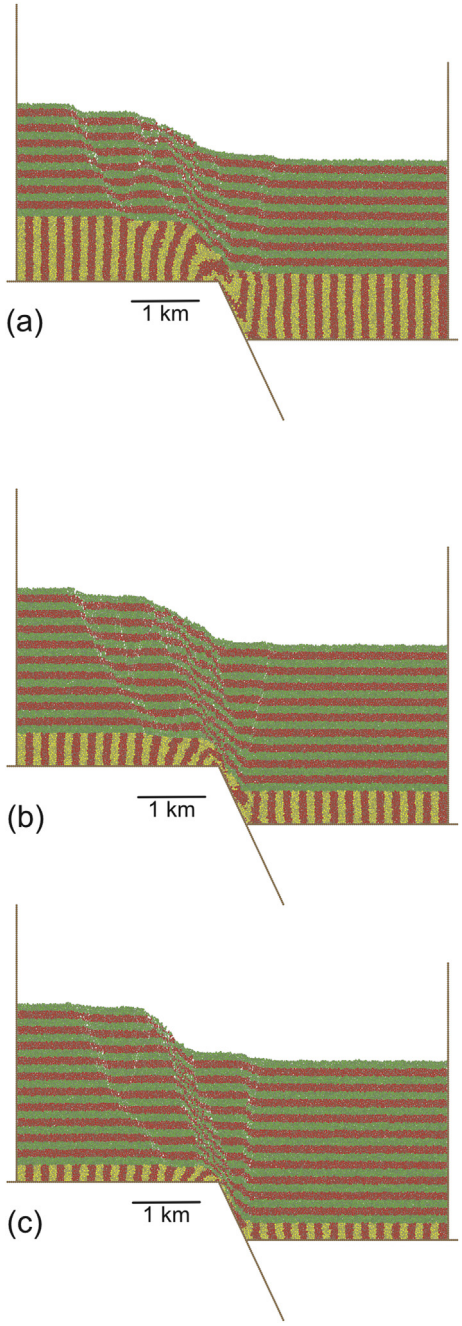

Fig. 7. Final geometries after 1000 m basement fault displacement for 3 experiments with a 65° basement fault and initial salt thicknesses of (a) 1000, (b) 500 and (c) 250 m respectively. Models run at the standard strain rate (c. 10^{15} s^{-1}). All other model parameters are identical. Note the production of salt welds and linkage of deformation in basement to cover with decreasing initial salt thickness.

basement fault and a salt layer which is initially 250, 500 and 1000 m thick. Models were run at the standard strain rate (c. 10^{15} s^{-1}), all other model parameters are identical to Experiment 1. These models show the clear influence of salt thickness on the style of linkage between basement and cover. For the model with a thick salt thickness (1000 m) the deformation in the basement is essentially decoupled from that in the cover (Fig. 7a). In this case, deformation in the cover is distributed and extends into the footwall. The model with a thin salt thickness (250 m) shows a very different style of linkage; here deformation is localised and bears a close relationship to the basement fault (Fig. 7c). In addition, it can be seen that welding is produced in this model in the region of the basement fault tip. For the intermediate salt thickness (500 m), linkage is transitional between these 2 end members (Fig. 7b).

One distinct advantage of the approach used here is the ability to visualise deformation, at the same resolution, both within the brittle cover and the ductile substrate, either through the deformed geometry of initially regular markers or through strain analysis. In many analogue studies deformation within the brittle cover is clearly visible, well-defined and analysed in some detail (e.g., Withjack and Callaway, 2000; Brun and Fort, 2011). While some analogue modelling studies have used plugs of viscous material (passive markers) to elucidate flow patterns within viscous layers (e.g., Cartwright et al., 2012), in most cases flow patterns are either unknown/unquantified (Dooley et al., 2003; McClay et al., 2003) or approximated using image processing techniques (PIV) where edge effects complicate the analysis (Warsitzka et al., 2015). However these, and other, techniques do allow visualisation of displacement/strain in 3D on model surfaces (e.g. Dooley et al., 2016). The approach used here allows us to much more clearly see the *internal* relationships between basement faulting and incremental deformation in the viscous substrate and frictional cover.

Clearly the approach and experiments presented in this paper are only a first step towards modelling salt and sediments in this discrete element model. These experiments lack several features which may be important in salt tectonics and which need to examined/added in future studies: firstly buoyancy is not included in these experiments, although recent studies have suggested that it may often be over-emphasised in analogue models (Allen and Beaumont, 2012) and will be subject of a further paper. This, and the relatively thick, strong cover used here, dampen any reactive rise of salt Secondly, differential loading by a tapering load, or a deltaic wedge growing over an underlying salt layer has a clear effect upon salt movement and deformation within the sedimentary cover (e.g., Cohen and Hardy, 1996; Gemmer et al., 2004). Also, in general syn-tectonic and post-tectonic sedimentation have been shown to have an important effect upon salt movement and resultant deformation (e.g., Warsitzka et al., 2015). Finally, these models have been run in 2D, while 3D effects are clearly important (Dooley et al., 2003). All these topics are subjects of ongoing research.

4. Conclusions

This paper has presented a discrete element model of a sedimentary section composed of a viscous substrate and a cohesive-frictional overburden, subject to boundary conditions appropriate to both thick and thin-skinned extension. Models can be scaled to geological timescales whilst retaining very low Reynolds numbers. With this parallelised numerical code, model runtimes are measured in days and are achievable using todays desktop workstations.

The numerical model has been applied to 3 examples involving extensional deformation, two of which are thick-skinned and one is thin-skinned. The results are similar to those seen both in nature and in analogue modelling (cf. Fig. 1a,b & c). Movement of the viscous substrate is the result of both Couette-type and Poiseuille-type flows (and combinations thereof), whilst deformation in the cover takes the form of discrete, dilational faults. These faults typically lose displacement towards, and tip out at, the cover-substrate interface. In addition, in models with a basement fault, the fault itself presents a growing and important no-slip boundary which significantly affects viscous flow. For the salt layer thickness used here, faults in the brittle sedimentary cover are, in general, unlinked or only soft-linked to any basement faulting. However, as the displacement on the basement normal fault increases, the salt layer thins significantly near the edge of the footwall block, and faults within the cover sequence are more closely related to the master normal fault via the attenuated salt layer.

As expected, much of the deformation observed within the viscous salt layer, and thus the frictional cover, is conditioned by (no-slip) boundary conditions. Deformation in the cover sequence is less affected by boundary conditions (and edge effects) with lower values of strain-

rate (or equivalently, salt viscosity) than with higher values of strain-rate. As a result, the distribution and style of deformation both in the mobile substrate and the overlying brittle cover can change significantly. In addition, initially thinner salt layers produce greater linking between the deformation in basement and cover.

Acknowledgements

Discussions with, and the patience of, many colleagues over many years is appreciated; particular thanks must go to Harvey Cohen and Dave Waltham for stimulating my interest in salt tectonics and, more generally, viscous flow many years ago. Additional input from Tim Dooley, Nestor Cardozo and Chris Jackson on earlier versions of this paper are most appreciated. Discrete element modelling was carried out using cdem2D by the author and strain analysis carried out using SSPX by Nestor Cardozo.

References

Abe, S., van Gent, H., Urai, J.L., 2011. DEM simulation of normal faults in cohesive materials. Tectonophysics 512, 12–21.

Allen, J., Beaumont, C., 2012. Impact of inconsistent density scaling on physical analogue models of continental margin scale salt tectonics. J. Geophys. Res. 117, B08103. http://dx.doi.org/10.1029/2012JB009227.

Baldwin, S., White, N., Muller, R.D., 2003. Resolving multiple rift phases by strain-rate inversion in the Petrel Sub-basin, northwest Australia. In: Hillis, R.R., Muller, R.D. (Eds.), The Evolution and Dynamics of the Australian Plate. Geological Society of Australia Special Publication 22 and Geological Society of America Special Paper 372, pp. 245–263.

Botter, C., Cardozo, N., Hardy, S., Lecomte, I., Escalona, A., 2014. From mechanical modeling to seismic imaging of faults: a synthetic workflow to study the impact of faults on seismic. Mar. Petrol. Geol. 57, 187–207.

Botter, C., Cardozo, N., Hardy, S., Lecomte, I., Paton, G., Escalona, A., 2016. Seismic characterisation of fault damage in 3D using mechanical and seismic modelling. Mar. Petrol. Geol. 77, 973–990.

Brun, J.P., Fort, X., 2011. Salt tectonics at passive margins: geology versus models. Mar. Petrol. Geol. 28, 1123–1145.

Cardozo, N., Allmendinger, R.W., 2009. SSPX: a program to compute strain from displacement/velocity data. Comput. Geosci. 35, 1343–1357.

Cartwright, J., Jaclson, M., Dooley, T., Higgins, S., 2012. Strain partitioning in gravity-driven shortening of a thick, multilayered evaporite sequence. In: In: Alsop, G.I., Archer, S.G., Hartley, A.J., Grant, N.T., Hodgkinson, R. (Eds.), 2012. Salt Tectonics, Sediments and Prospectivity. Geological Society, London, vol. 363. Special Publications, pp. 449–470.

Chapman, B., Jost, G., van der Pas, R., 2007. Using OpenMP: Portable Shared Memory Parallel Programming. The MIT Press.

Cohen, H.A., Hardy, S., 1996. Numerical modelling of stratal architectures resulting from differential loading of a mobile substrate. In: In: Alsop, G.I., Blundell, D.J., Davison, I. (Eds.), Salt Tectonics, vol. 100. Geological Society Special Publication, London, pp. 265–273.

Crook, A., Wilson, S., Yu, J., Owen, D., 2006. Predictive modelling of structure evolution in sandbox experiments. J. Struct. Geol. 28, 729–744.

Cundall, P.A., Strack, O.D.L., 1979. A discrete numerical model for granular assemblies. Geotechnique 29, 47–65.

Dean, S., 2014. Tectonic and Gravitational Fold and Thrust Belts: Insights from Discrete Element Simulations and Galicia Bank Ocean-continent Transition Zone: New Seismic Reflection Constraints. PhD Thesis. Rice University.

Dean, S., Morgan, J.K., Brandenburg, J.P., 2015. Influence of mobile shale on thrust faults: insights from discrete element simulations. AAPG (Am. Assoc. Pet. Geol.) Bull. 99 (03), 403–432.

Demercian, S., Szatmari, P., Cobbold, P.R., 1993. Style and pattern of salt diapirs due to thin-skinned graviational gliding, Campos and Santos basins. offshore Brazil: Tectonphysics 228, 393–433.

Dooley, T.P., McClay, K.R., Pascoe, R., 2003. 3D analogue models of variable displacement extensional faults: applications to the Revfallet fault systems, Mid-Norway. In: In: Nieuland, D.A. (Ed.), New Insights into Structural Interpretation and Modelling, vol. 212. Geological Society of London Special Publication, pp. 151–167.

Dooley, T.P., Jackson, M.P.A., Hudec, M.R., 2007. Initiation and growth of salt-based thrustbelts on passive margins: results from physical models. Basin Research 19, 165–177.

Dooley, T.P., Hudec, M.R., Carruthers, D., Jackson, M.P.A., Luo, G., 2016. The effects of base-salt relief on salt flow and suprasalt deformation patterns — Part 1: flow across simple steps in the base of salt. Interpretation 5 (1), SD1–SD23. https://doi.org/10.1190/INT-2016-0087.1.

Duffy, O.B., Gawthorpe, R.L., Docherty, M., Brocklehurst, S.H., 2013. Mobile evaporite controls on the structural style and evolution of rift basins. Basin Res. 25, 310–330.

Egholm, D.L., Sandiford, M., Clausen, O.R., Nielsen, S.B., 2007. A new strategy for discrete element numerical models: 2. Sandbox applications. J. Geophys. Res. 112, B05204. http://dx.doi.org/10.1029/2006JB004558.

Ferrill, D.A., Morris, A.P., McGinnis, R.N., Smart, K.J., Wigginton, S.S., Hill, N.J., 2017. Mechanical stratigraphy and normal faulting. Journal of Structural Geology, v. 94 275–302. ISSN 0191-8141. https://doi.org/10.1016/j.jsg.2016.11.010. http://www.sciencedirect.com/science/article/pii/S0191814116301985.

Finch, E., Hardy, S., Gawthorpe, R.L., 2004. Discrete element modelling of extensional fault-propagation folding above rigid basement fault blocks. Basin Res. 16, 489–506.

Ge, H., Jackson, M.P.A., Vendeville, B.C., 1997. Kinematics and dynamics of salt tectonics driven by progradation. AAPG (Am. Assoc. Pet. Geol.) Bull. 81, 398–423.

Ge, Z., Gawthorpe, R.L., Rotevatn, A., Thomas, M.B., 2016. Impact of normal faulting and pre-rift salt tectonics on the structural style of salt-influenced rifts: the Late Jurassic Norwegian Central Graben, North Sea. Basin Res. http://dx.doi.org/10.1111/bre.12219.

Gemmer, L., Ings, S., Medvedev, S., Beaumont, C., 2004. Salt tectonics driven by differential sediment loading: stability analysis and finite element experiments. Basin Res. 16, 199–218.

Gemmer, L., Beaumont, C., Ings, S., 2005. Dynamic modelling of passive margin salt tectonics: effects of water loading, sediment properties and sedimentation patterns. Basin Res. 2005 (17), 383–402. http://dx.doi.org/10.1111/j.1365-2117.2005.00274.x.

Gray, J.P., Monaghan, J.J., 2004. Numerical modelling of stress fields and fracture around magma chambers. J. Volcanol. Geoth. Res. 135, 259–283.

Hardy, S., 1994. Mathematical Modelling of Sedimentation in Active Tectonic Settings. PhD Thesis. Royal Holloway University of London.

Hardy, S., 2008. Structural evolution of calderas: insights from two-dimensional discrete element simulations. Geology 36, 927–930.

Hardy, S., 2011. Cover deformation above steep, basement normal faults: insights from 2D discrete element modeling. Mar. Petrol. Geol. 28, 966–972.

Hardy, S., 2015. The Devil truly is in the detail. A cautionary note on computational determinism: implications for structural geology numerical codes and interpretation of their results. Interpretation 3 (4). http://dx.doi.org/10.1190/INT-2015-0052.1. SAA29–SAA35.

Hardy, S., 2016. Does shallow dike intrusion and widening remain a possible mechanism for graben formation on Mars? Geology 44, 107–110. http://dx.doi.org/10.1130/G37285.1.

Hardy, S., McClay, K., Muñoz, J.A., 2009. Deformation and fault activity in space and time in high-resolution numerical models of doubly vergent thrust wedges. Mar. Petrol. Geol. 26, 232–248. http://dx.doi.org/10.1016/j.marpetgeo.2007.12.003.

Hodgson, N.A., Farnsworth, J., Fraser, A.J., 1992. Salt-related tectonics, sedimentation and hydrocarbon plays in the central graben, North Sea, UKCS. In: In: Hardman, R.F.P. (Ed.), Exploration Britain: Geological Insights for the Next Decade, vol. 67. Geol. Soc. Spec. Publ., pp. 31–63.

Holohan, E.P., Schopfer, M.P.J., Walsh, J.J., 2011. Mechanical and geometric controls on the structural evolution of pit crater and caldera subsidence. J. Geophys. Res. 116, B07202 doi:1029/2010JB008032.

Horsfield, W.T., 1977. An experimental approach to basement-controlled faulting. Geol. Mijnbouw 56, 363–370.

Jackson, C.A.-L., Lewis, M.M., 2016. Structural style and evolution of a salt-influenced rift basin margin; the impact of variations in salt composition and the role of polyphase extension. Basin Res. 28, 81–102. http://dx.doi.org/10.1111/bre.12099.

Jackson, M.P.A., Talbot, C.J., 1994. Advances in salt tectonics. In: Hancock, P.L. (Ed.), Continental deformation. International Union of Geological Sciences, pp. 159–179.

Jackson, M.P.A., Vendeville, B.C., 1994. Regional extension as a geological trigger for diapirism. Geol. Soc. Am. Bull. 106, 57–73.

Kaus, B.J.P., Podladchikov, Y.Y., 2001. Forward and reverse modelling of the three-dimensional viscous Rayleigh-Taylor instability. Geophys. Res. Lett. 28, 11095–11098.

Koyi, H., 1996. Salt flow by aggrading and prograding overburdens. In: In: Alsop, G.I., Blundell, D.J., Davison, I. (Eds.), Salt Tectonics, vol. 100. Geological Society of London Special Publication, pp. 243–258.

Last, N.C., 1988. Deformation of a sedimentary overburden on a slowly creeping substratum. In: Swoboda (Ed.), Numerical Methods in Geomechanics (Innsbruck 1988). Balkema, Rotterdam, pp. 577–585.

Lewis, M.M., Jackson, C.A.-L., Gawthorpe, R.L., 2013. Salt-influenced normal fault growth and forced folding: the stavanger fault system, North Sea. J. Struct. Geol. 54, 156–173.

McClay, K.R., 1990. Extensional fault systems in sedimentary basins: a review of analogue model studies. Mar. Petrol. Geol. 7, 206–233.

McClay, K.R., Dooley, Tim, Zamora, G., 2003. Analogue models of delta systems above mobile shales. In: In: Van Rensbergen, P., Morley, C., Hillis, R., Cartwright, J. (Eds.), Geological Society of London, vol. 216. Special Publication, pp. 411–428.

Marsh, N., Imber, J., Holdsworth, R.E., Brockbank, P., Ringrose, P., 2010. The structural evolution of the Halten Terrace, offshore Mid-Norway: extensional fault growth and strain localisation in a multi-layer brittle-ductile system. Basin Res. 22 (2), 195–214.

Marton, L.G., Tari, G.C., Lehmann, C.T., 2000. Evolution of the Angolan passive margin, West Africa, with emphasis on post-salt structural styles. In: Webster, M., Talwani, M. (Eds.), Atlantic Rifts and Continental Margins: American Geophysical Union Geophysical Monograph. vol.115. pp. 129–149.

Mora, P., Place, D., 1993. A lattice solid model for the non-linear dynamics of earthquakes. Int. J. Mod. Phys. C 4, 1059–1074.

Nollet, S., Kleine Vennekate, G.J., Giese, S., Vrolijk, P., Urai, J.L., Zeigler, M., 2012. Localization patterns in sandbox-scale numerical experiments above a normal fault in basement. J. Struct. Geol. 39, 199–209.

Oger, L., Savage, S.B., Corriveau, D., Sayed, M., 1998. Yield and deformation of an assembly of disks subject to a deviatoric stress loading. Mech. Mater. 27, 189–210.

Pichel, L.M., Finch, E., Huuse, M., Redfern, J., 2017. The influence of shortening and sedimentation on rejuvenation of salt diapirs: a new Discrete-Element Modelling approach. J. Struct. Geol. 104, 61–79.

Podladchikov, Y., Talbot, C., Poliakov, A.N.B., 1993. Numerical models of complex

diapirs. Tectonophysics 228, 189–198.
Poliakov, A.N.B., Podladchikov, Y., Talbot, C., 1993. Initiation of salt diapirs with frictional overburdens: numerical experiments. Tectonophysics 228, 199–210.
Richardson, N.J., Underhill, J.R., Lewis, G., 2005. The role of evaporite mobility in modifying subsidence patterns during normal fault growth and linkage, Halten Terrace, Mid-Norway. Basin Res. 17, 203–223.
Rowan, M., Trudgil, B.D., Fiduk, J.C., 2000. Deep-water, salt-cored foldbelts: lessons from the Mississippi fan and perdido foldbelts, northern Gulf of Mexico. In: Webster, M., Talwani, M. (Eds.), Atlantic Rifts and Continental Margins: American Geophysical Union Geophysical Monograph. vol.115. pp. 173–191.
Saltzer, S.D., Pollard, D.D., 1992. Distinct element modeling of structures formed in sedimentary overburden by extensional reactivation of basement normal faults. Tectonics 11, 165–174.
Schultz-Ela, D., Walsh, P., 2001. Modeling of grabens extending above evaporites in canyonlands national park, Utah. J. Struct. Geol. 24, 247–275.
Schultz, R.A., 1996. Relative scale and the strength and deformability of rock masses. J. Struct. Geol. 18, 1139–1149.
Stewart, S.A., 2007. Salt tectonics in the North Sea Basin: a structural style template for seismic interpreters. In: In: Ries, A.C., Butler, R.W.H., Graham, R.H. (Eds.), Deformation of the Continental Crust: the Legacy of Mike Coward, vol.272. Geol. Soc. Spec. Publ., pp. 361–396.
Stewart, S., Coward, M.P., 1995. Synthesis of salt tectonics in the southern North Sea. Mar. Petrol. Geol. 12 (no. 5), 457–475. http://dx.doi.org/10.1016/0264-8172(95)91502-G.
Stewart, S.A., Harvey, M.J., Otto, S.C., Weston, P.J., 1996. Influence of salt on fault geometry: examples from the UK salt basins. In: In: Alsop, G.I., Blundell, D.J., Davison, I. (Eds.), Salt Tectonics, vol. 100. Geol. Soc. Spec. Publ., pp. 175–202.
Stewart, S.A., Ruffell, A.H., Harvey, M.J., 1997. Relationship between basement-linked and gravity-driven fault systems in the UKCS salt basins. Mar. Petrol. Geol. 14, 581–604.
Strayer, L.M., Erickson, S.G., Suppe, J., 2004. Influence of growth strata on the evolution of fault-related folds: distinct-element models. In: In: McClay, K. (Ed.), Thrust Tectonics and Hydrocarbon Systems, vol.82. American Association of Petroleum Geologists Memoir, pp. 413–437.
Tari, G.C., Ashton, P.R., Coterill, K.L., Molnar, J.S., Sorgenfrei, M.C., Thompson, P.W.A., Valasek, D.W., Fox, J.F., 2002. Are west Africa deepwater salt tectonics analogues to the Gulf of Mexico? Oil Gas J. 4, 73–81.
Thompson, N., Bennett, M.R., Petford, N., 2010. Development of characteristic volcanic debris avalanche deposit structures: new insights from distinct element simulations. J. Volcanol. Geoth. Res. 192, 191–200.
Turcotte, D.L., Schubert, G., 1982. Geodynamics - Applications of Continuum Physics to Geological Problems. Wiley, New York, pp. 450.
Valencia, D.C.C., Botter, C., Hardy, S., Cardozo, N., 2016. Seismic imaging of salt-influenced compressional folds. In: 78th EAGE Conference and Exhibition 2016, Vienna 2016.
van Gent, H.W., Holland, M., Urai, J.L., Loosveld, R., 2010. Evolution of fault zones in carbonates with mechanical stratigraphy - insights from scale models using layered cohesive powder. J. Struct. Geol. 32, 1375–1391.
Vendeville, B.C., 1988. Scale-models of basement induced-extension. C. R. Acad. Sci. 307, 1013–1019.
Vendeville, B.C., Jackson, M.P.A., 1992. The rise of diapirs during thin-skinned extension. Mar. Petrol. Geol. 9, 331–353.
Waltham, D., 1997. Why does salt start to move? Tectonophysics 282, 117–128. https://doi.org/10.1016/S0040-1951(97)00215-1.
Warsitzka, M., Kley, J., Kukowski, N., 2015. Analogue experiments of salt flow and pillow growth due to basement faulting and differential loading. Solid Earth 6, 9–31. http://dx.doi.org/10.5194/se-6-9-2015.
Withjack, M.O., Callaway, S., 2000. Active normal faulting beneath a salt layer: an experimental study of deformation patterns in the cover sequence. AAPG (Am. Assoc. Pet. Geol.) Bull. 84 (No. 5), 627–651 May 2000.
Worrall, D.M., Snelson, S., 1989. Evolution of the northern Gulf of Mexico, with emphasis on Cenozoic growth faulting and the role of salt. In: Bally, A.W., Palmer, A.R. (Eds.), The Geology of North America: an Overview. Geological Society of America, The Geology of North America, Boulder, Colorado, pp. 97–138 vol. A.
Wu, S., Bally, A., Cramez, C., 1990. Allochthonous salt, structure and stratigraphy of the north-eastern Gulf of Mexico. Part II: Structure. Mar. Petrol. Geol., vol.7, 334–370.